XX IMEKO World Congress
Metrology for Green Growth
September 9–14, 2012, Busan, Republic of Korea

COMPARISON OF MILIGRAM SCALE DEADWEIGHT FORCES TO ELECTROSTATIC FORCES

Sheng-Jui Chen, Sheau-Shi Pan and Yi-Ching Lin

Center for Measurement Standards, Industrial Technology Research Institute, Hsinchu, Taiwan 300, R.O.C.
Electronic address: sj.chen@itri.org.tw

Abstract: This paper presents a comparison of milligram scale deadweight forces to electrostatic forces that is generated from an electrostatic sensing & actuating force measurement system recently built in Center for Measurement Standards, Industrial Technology Research Institute (CMS/ITRI). In the first section, we briefly introduce the electrostatic sensing and actuating force measurement system, and then we describe the experimental setup for the comparison and the results. Finally, we give a discussion and outlook.

Keywords: deadweight force, electrostatic force, electrostatic actuation, capacitive position sensing, force balance.

1. INTRODUCTION

Micro- and nano-force measurement is of great interest in recent years among several national measurement institutes (NMIs) [1-5]. Center for Measurement Standards (CMS) of Industrial Technology Research Institute (ITRI) has established a force measurement system based on electrostatic sensing & actuation techniques. The system is capable of measuring vertical forces up to 200 μN using force balance method and mainly consists of a flexure stage, a three-electrode capacitor and a digital controller [6]. The schematic drawing of the system is shown in figure 1.

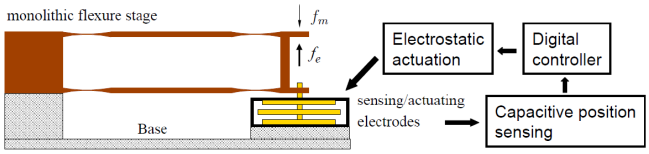

Figure 1: The schematic drawing of the force measurement system.

The three-electrode capacitor is used simultaneously as a capacitive position sensor and an electrostatic force actuator. The position of the center electrode is detected by comparing the top and bottom capacitors formed by the three electrodes using an inductive-capacitive resonant bridge circuit. The position detection is performed at a radio frequency (RF), say, 100 kHz, a frequency depending on the capacitance values and the design of the sensing bridge circuit. For electrostatic force actuation, the top and bottom electrodes are applied with two high voltage, audio frequency sinusoidal signals to generate a compensation electrostatic force f_e to balance the force under measurement f_m. The balance condition $f_m = -f_e$ is maintained by the digital controller by keeping the flexure stage at its zero deflection position. Some parts of the force measurement system were upgraded. A new design of copper-beryllium flexure stage was installed in the system, which has a counter weight balance mechanism and a lower stiffness of 13.08 N/m. A new set of gold-plated, polished electrodes was assembled as a three-electrode capacitor and put into operation. The capacitance gradient for the new three-electrode capacitor was measured.

2. EXPERIMENTAL SETUP

In this experiment, the compensation electrostatic force is compared to the deadweight force by weighing a weight with the electrostatic sensing and actuating force measurement system.

Deadweight force: We used five wire weights with nominal mass values and shapes of 1 mg-triangle, 2 mg-square, 5 mg-pentagon and 10 mg-triangle to generate vertical downward forces. These weights meet the metrological requirement of the OIML class E_1 and were calibrated against standard weights using mass comparator balance. The calibration results are compiled in table 1. The deadweight forces can be derived from the calibrated mass values and the local acceleration of gravitation g = 9.78914 m/s^2 as $f_w = m\,(1 - \rho_a / \rho_w)\,g$, where ρ_a and ρ_w are densities of the air and the weight respectively. These weights were loaded and unloaded by a DC motor actuated linear translation stage.

Table 1: Mass calibration result.

Nominal mass (mg)	Conventional mass (mg)	Uncertainty, 95% confidence (mg)
1	1.00096	0.0003
2	2.00116	0.0003
5	5.00124	0.00065
10	10.0021	0.00048

Electrostatic force: As shown in figure 2, the compensation electrostatic force f_e generated by the force measurement system is determined by the following equation

$$f_e = \frac{1}{2} S_1 V_1^2 + \frac{1}{2} S_2 V_2^2 \quad , \qquad (1)$$

where S_1, S_2 are the capacitance gradients of the top and the bottom capacitors C_1, C_2 and V_1, V_2 are voltage potentials

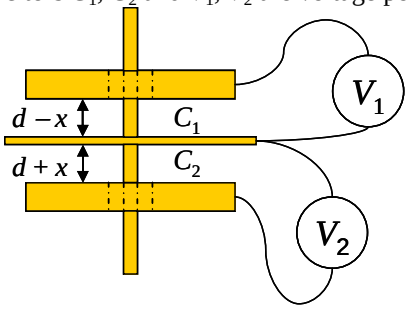

Figure 2: Three-electrode capacitor for electrostatic force actuation.

between the top and the bottom capacitors respectively. Using the parallel-plate capacitor as the model for capacitor C_1 and C_2, then the capacitance gradients S_1 and S_2 can be expressed as (with d being the gap distance between electrodes when the center electrode is vertically centered)

$$S_1(x) = \frac{dC_1}{dx} \cong S_0 \left[1 + 2\frac{x}{d} + 3\frac{x^2}{d^2} + 4\left(\frac{x}{d}\right)^3 + 5\left(\frac{x}{d}\right)^4 + \cdots \right] \qquad (2)$$

$$S_2(x) = \frac{dC_2}{dx} \cong S_0 \left[-1 + 2\frac{x}{d} - 3\left(\frac{x}{d}\right)^2 + 4\left(\frac{x}{d}\right)^3 - 5\left(\frac{x}{d}\right)^4 + \cdots \right], \qquad (3)$$

where d is the gap distance between electrodes when the center electrode is vertically centered. The electrostatic force can be written as

$$f_e = \frac{1}{2} S_0 (V_1^2 - V_2^2) + \frac{x}{d} S_0 (V_1^2 + V_2^2) \cdot \qquad (4)$$

The voltage V_1 and V_2 contain the RF detection signal $V_d \sin\omega_d t$, audio frequency high voltage actuation voltages $V_{a1}\sin\omega_a t$, $V_{a2}\sin\omega_a t$ and the electrodes' surface potentials v_{s1}, v_{s2}, namely

$$V_1 = V_d \sin\omega_d t + V_{a1} \sin\omega_a t + v_{s1} \qquad (5)$$

$$V_2 = V_d \sin\omega_d t + V_{a2} \sin\omega_a t + v_{s2} \cdot \qquad (6)$$

The high voltage actuation signals are provided by a full range ±10 V 16-bit resolution digital-to-analog converter within the digital controller and an ultra low noise high voltage amplifier. To make the electrostatic force linearly proportional to a control voltage v_c, we set

$$V_{a1} = A_1 (V_b + v_c) \qquad (7)$$

$$V_{a2} = A_2 (V_b - v_c) , \qquad (8)$$

where A_1, A_2 are amplification factors of the high voltage amplifier. The term V_b is a constant and determined by the value of S_0 and the upper limit of the force measurement range. Taking the gain difference between channels of high voltage amplifier, substituting equation (5)-(8) for V_1 and V_2 in equation (4), we obtain an equation for describing the electrostatic force f_e

$$f_e = S_0 A_0^2 V_b v_c + S_0 A_0^2 (a+b)(v_c^2 + V_b^2) + S_0 (v_s^2 + b V_d^2) \quad , \qquad (9)$$
$$+ (\text{ac terms})$$

where a is the gain difference fraction, i.e. $a=(A_1-A_2)/(A_1+A_2)$, A_0 is the mean gain factor, b is the offset fraction x/d, $v_s^2 = (v_{s1}^2 - v_{s2}^2)/2$ and v_c is the control voltage. The high frequency AC terms at audio and RF frequencies can be omitted because they cause only negligible ac displacement modulations on the flexure stage.

Parameter a can be tuned to very close to zero by adjusting the gain of the DAC within a software program. After the tuning, parameter a was measured to be smaller than 5×10^{-5} contributing a negligible force uncertainty. Instead of using the optical interferometer, the position of the center electrode is measured by the difference between C_1 and C_2 with a differential capacitance bridge circuit [6]. Hence, the position of the center electrode can be brought to the vertical center position by nulling the output of the differential capacitance bridge circuit. With commercially available optical interferometer, the offset adjustment could be quite difficult and ambiguous. The effect of parameter (a+b) can be tested by setting v_c=0, modulating V_b with a square wave profile and observing the displacement signal of the flexure stage. For V_b=2.0, we did not observe the displacement due to the modulated V_b.

The remaining factors S_0, v_c and v_s dominate the uncertainty of the electrostatic force f_e. The capacitance gradient S_0 was measured using a weight of 1 mg and a set of optical interferometer. The weight of 1 mg was cyclically loaded and unloaded to the system by a motorized linear stage to produce a deflection modulation. The deflection was measured by the optical interferometer and the corresponding capacitance variation was measured by a calibrated precision capacitance bridge. To reduce the effect from seismic noise and drift noise from the optical interferometer or the flexure stage itself, both deflection Δx and capacitance variation ΔC are measured from the difference between average values of mass loaded data and two adjacent mass unloaded data. The capacitance gradient S_0 is just the ratio of $\Delta x/\Delta C$ which is shown in figure 6. The capacitance gradient has a mean value of $S_0 = 2.876\times10^{-8}$ F/m and a standard deviation of $\sigma_S = 0.008\times10^{-8}$ F/m. Therefore, the standard uncertainty of the capacitance gradient is $u(S_0) = \frac{\sigma_S}{\sqrt{N}} = 4\times10^{-12}$ F/m with N = 369 in this measurement. The uncertainty $u(v_c)$ of control voltage v_c is calculated using the DAC resolution of 0.3 mV as $u(v_c) = 0.3/(2\sqrt{3}) = 0.088\,\text{mV}$ which contributes 1 nN. For the surface potential noise v_s, the current actuation scheme prevents the surface potential effect from being coupled to and amplified by the control voltage v_c as in the previous

electrostatic actuation scheme [6] Sv_cv_s. The surface potential is reported to range from 20 mV to 180 mV [7, 8]. Taking v_s = 0.18 V for example and $S = 2.876 \times 10^{-8}$ F/m, the surface potential induced electrostatic force is about 0.9 nN.

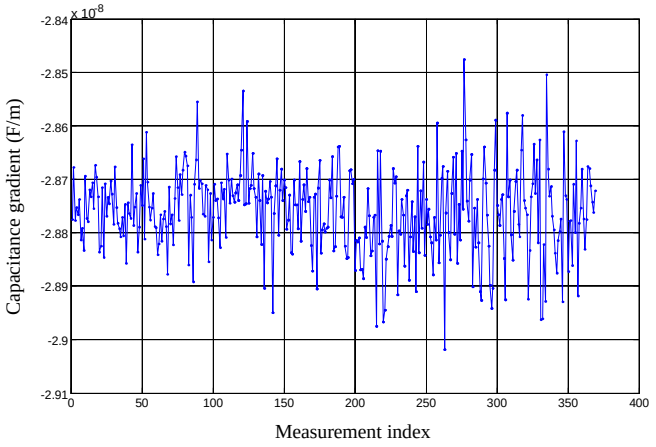

Figure 3: Capacitance gradient calculated from $\Delta C/\Delta x$. The mean capacitance gradient S_0 = 2.876×10^{-8} F/m, standard deviation σ_S = 0.008×10^{-8} F/m and standard deviation of the mean $\frac{\sigma_S}{\sqrt{N}} = 4\times10^{-12}$ F/m (N = 369 in this measurement).

Null deflection control: The force under measurement f_m is balanced by f_e by the null deflection control. Figure 4 shows the block diagram of the null deflection control. The transfer functions of the main components, namely the flexure stage, capacitive position sensor, loop filter and the electrostatic force actuator, are represented by G, H, D and A respectively. The term x_n represents a deflection noise which may be contributed by the seismic vibration noise and the thermal noise of the flexure stage itself. The relation between f_e and f_m was derived to be

$$F_e(s) = -\frac{HDA}{1+T(s)} X_s(s) - \frac{T(s)}{1+T(s)} F_m(s), \qquad (10)$$

where $T(s) = GDHA$ is the open-loop transfer function of the control system, and $F_e(s)$, $X_s(s)$ and $F_m(s)$ are Laplace transform of f_e, x_s and f_m respectively.

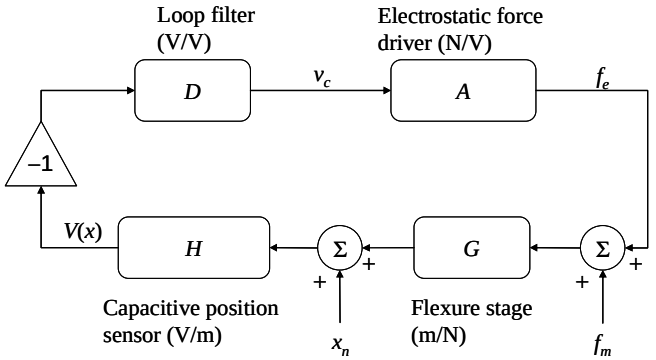

Figure 4: Block diagram of the null deflection control some noise sources are omitted for simplicity.

Within the control bandwidth, i.e. for $T(s)$ >> 1, the relation between f_e and f_m can be approximated as

$$f_e = -(kx_n + f_m), \qquad (11)$$

where k is the stiffness of the flexure stage. Equation (11) shows that the null deflection control automatically generates a compensation force f_e to balance the force under measurement f_m. To reduce influence form the noise x_n, f_m is measured in a short period of time by comparing $f_e(t_0)$ before f_m is applied and $f_e(t_1)$ after f_m is applied:

$$\Delta f_e = f_e(t_1) - f_e(t_0) = -k[x_n(t_1) - x_n(t_0)] - f_m$$

thus

$$f_m = -\Delta f_e - kx_{nt}. \qquad (12)$$

The term x_{nt} represent the temporal variation of x_n during the measurement time frame. From one deflection measurement data taken for 8-hr, using a time frame of 300 s to evaluate x_{nt}, we obtained a standard deviation of 0.33 nm for x_{nt}. With the measured k of 13.0 N/m, the standard deviation of the x_{nt} equivalent force noise is 4.3 nN.
Table 2 listed the main sources of uncertainty of the measured f_m.

Table 2: Uncertainty budget for measured f_m

Source of uncertainty	Standard uncertainty (N)
Capacitance gradient S_0	$1.4\cdot10^{-4}\Delta f_e$
16-bit DAC resolution	$1\cdot10^{-9}$
Surface potential v_s	$1.8\cdot10^{-9}$
Displacement noise x_{nt}	$4.3\cdot10^{-9}$
Combined standard uncertainty: $u(f_m) = \sqrt{(4.8\cdot10^{-9})^2 + (1.4\cdot10^{-4}\Delta f_e)^2}$ N	

Weighing process: Each weight was loaded for 100 seconds and unloaded for 100 seconds. The compensation electrostatic force was calculated from the control voltage v_c. Figure 5 shows the control voltage v_c acquired during one weighing cycle. The voltage difference Δv_c was determined from one weight loaded segment and its two adjacent weight unloaded segments as

$$\Delta v_c = v_{cB} - \frac{v_{cA1}}{2} - \frac{v_{cA2}}{2}. \qquad (5)$$

The weighing cycle was repeated for a long period of time in order to evaluate the stability and uncertainty of the system.

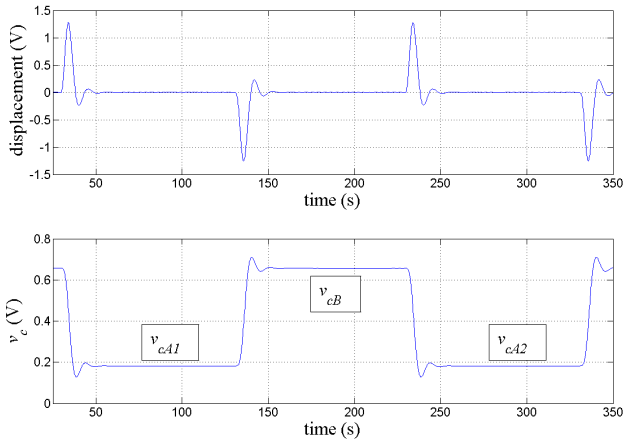

Figure 5: The capacitive displacement and control voltage v_c during one weighing cycle.

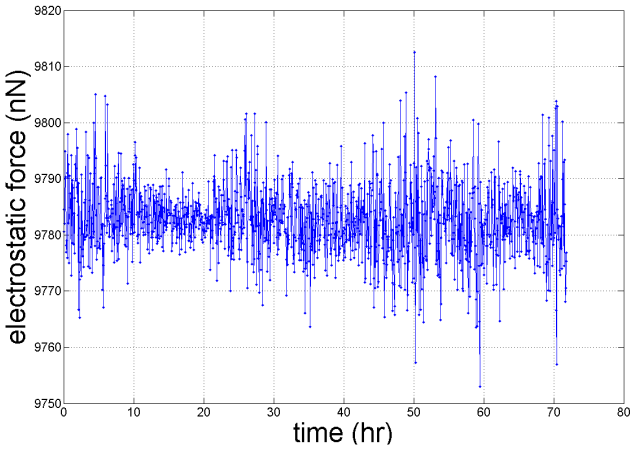

Figure 6: A data run for 1 mg weighing.

3. RESULTS

Figures 6 shows the result of one weighing run for the weight of 1 mg. The measurement was taken for three days. For this run, the electrostatic force is f_e = (9,782.6 ± 6.7) nN, where the given uncertainty is the one standard deviation. The deadweight forces produced from the weights are estimated as $f_w = mg\,(1-\rho_{air}/\rho_{mass})$, where the air buoyancy is taken into consideration. The comparison results are compiled in table 3.

Table 3: Comparison results, unit in nN.

	1 mg	2 mg	5 mg	10 mg
f_w	9797.1±2.9	19586.7±2.9	48950.5±6.4	97897.3±4.7
f_e	9782.6±6.7	19527.0±4.1	48751.4±8.2	97886.4±16.5
f_e-f_w	-14.5	-59.7	-199.1	-10.9

In general, the electrostatic force has a smaller value than the deadweight force. For comparisons of weights 1 mg and 10 mg, the force differences defined as f_e-f_w are similar and close to 10 nN, and they both are in triangle shapes with similar dimensions. For comparisons of the weight 2 mg and 5 mg, the force differences are rather larger, and they are in shapes of square and pentagon, respectively. The weight of 5 mg has the largest force difference of about 200 nN (20 μg), and it is the biggest weight in terms of wire length and shape area dimensions. A possible explanation for this force difference is that there might be some extra electrostatic or magnetic force between the weight and its surroundings. Due to the size of the weight 5 mg, it has the shortest distances to and possibly experiences the strongest electrostatic/magnetic interactions with its surroundings.

4. DISCUSSION AND OUTLOOK

The force measurement system based on the electrostatic sensing and actuation techniques has been built and upgraded. The system is enclosed by a vacuum chamber which resides on a passive low frequency vibration isolation platform. The voltage actuation scheme has been modified to allow the decoupling between the surface potential v_s and the actuation voltage leading to a reduction in the drift and bias of the compensation electrostatic force. The system is stable over a long period of time. However, the cause of the extra electrostatic/magnetic force observed in the weighing test is still unclear and investigation to that is underway. A new design of the apparatus's housing is being fabricated, it was designed to isolate most of the apparatus from its surroundings and expose only the force loading area. In addition, other parameters such as alignment factors, the capacitance gradient and its frequency dependence will also be re-verified and further studied to find out the cause for the force difference.

5. REFERENCES

[1] Newell D B, Kramar J A, Pratt J R, Smith D T and Williams E R, "The NIST microforce realization and measurement project", *IEEE Trans. Instrum. Meas.* **52** (2003) 508

[2] Kim M-S, Choi J-H, Park Y-K and Kim J-H, "Atomic force microscope cantilever calibration device for quantified force meterology at micro- or nano-scale regime: the nano force calibrator (NFC)", *Metrologia* **43** (2006) 389-395

[3] Leach R, Chetwynd D, Blunt L, Haycocks J, Harris P, Jackson K, Oldfield S and Reilly S, "Recent advances in traceable nanoscale dimension and force metrology in the UK", *Meas. Sci. Technol.* **17** (2006) 467-476

[4] Choi J-H, Kim M-S, Park Y-K and Choi M-S, "Quantum-based mechanical force realization in piconewton range", *Appl. Phys. Lett.* **90** (2007) 073117

[5] Nesterov V, "Facility and methods for the measurement of micro and nano forces in the range below 10-5 N with a resolution of 10^{-12} N (development concept)", *Meas. Sci. Technol.* **18** (2007) 360-366

[6] S-J Chen and S-S Pan, "A force measurement system based on an electrostatic sensing and actuating technique for calibrating force in a micronewton range with a resolution of nanonewton scale", *Meas. Sci. Technol.*, **22** (2011), 045104

[7] J.R. Pratt and J.A. Kramar, "SI realization of small forces using an electrostatic force balance", Proc. 18th IMEKO World Congress, (17-22 September 2006, Rio de Janeiro, Brazil)

[8] S.E. Pollack, S. Schlamminger and J.H. Gundlach, "Temporal extent of surface potentials between closely spaced metals", *Phys. Rev. Lett.* **101** (2008), 071101